Article

Experimental and Theoretical Investigations of *Argania spinosa*'s Extracts on the Antioxidant Activity and Mild Steel Corrosion's Inhibition in 1 M HCl

Hamid Laaroussi [1], Abdelouahad Aouniti [1], Ouafae Mokhtari [2], Baraa Hafez [3], Ryan Adnan Sheikh [4], Manal Y. Sameeh [5], Manal M. Khowdiary [5], Suliman A. Alderhami [6], Ahmed A. Elhenawy [6,7,*], Mohamed El Azzouzi [1], Ilyesse Rahhou [8], Chaouki Belbachir [9], Belkheir Hammouti [1], Taibi Ben Hadda [1] and Hicham Elmsellem [1,*]

1   Laboratory of Applied Chemistry and Environment (LCAE), Sciences Faculty, Oujda 60000, Morocco
2   Laboratory of the Improvement of Agricultural Production, Biotechnology and Environment, Sciences Faculty, Oujda 60000, Morocco
3   Department of Pharmaceutical Sciences, College of Pharmacy and Health Sciences, Ajman University, Ajman P.O. Box 346, United Arab Emirates
4   Biochemistry Department, Faculty of Science, King Abdulaziz University, Jeddah 21589, Saudi Arabia
5   Chemistry Department, Faculty of Applied Science, Umm El Qura Branch, Makkah 24211, Saudi Arabia
6   Department of Chemistry, Faculty of Science and Arts in Al-Mukhwah, Al-Baha University, Al Bahah 65311, Saudi Arabia
7   Chemistry Department, Faculty of Science, Al-Azhar University, Nasr City, Cairo 11884, Egypt
8   Higher Institute of Nursing Professions and Health Techniques (ISPITSO), Oujda 63303, Morocco
9   Laboratoire Régional de Recherches et d'Analyses de Berkane—ONSSA, Qualipole Alimentaire, Agropole de Berkane, Berkane 63303, Morocco
*   Correspondence: elhenawy_sci@hotmail.com (A.A.E.); h.elmsellem@gmail.com (H.E.)

Abstract: The aim of the present research is the evaluation of the extraction process effect on the chemical composition, the antioxidant activities, and the mild steel corrosion inhibition ability of *Argania spinosa*'s extracts (alimentary oil (AO) and hexanic extract of roasted almonds (HERA)). The chemical composition revealed that both extracts have the same major compounds: Palmitic, linoleic, and stearic acids, with their order slightly different. Electrochemical impedance spectroscopy (EIS), weight loss measurements, and polarization curves were used to estimate AO and HERA's mild steel corrosion's inhibition capacity. Based on these three methods, AO registered, respectively, 81%, 87%, and 87% inhibition efficiency while HERA registered 78%, 84%, and 82% inhibition efficiency. The antioxidant activity of AO and HERA was examined in parallel with standard antioxidants (gallic acid and quercetin) using two assays: DPPH* scavenging assay and ferric reducing antioxidant power assay (FRAP). AO had less EC_{50} in both techniques (DPPH*: 3559.08 ± 161.75 µg/mL; FRAP 1288.58 ± 169.21 µg/mL) than HERA (DPPH*: 3621.43 ± 316.05 µg/mL; FRAP 1655.86 ± 240.18 µg/mL). Quantum chemical and molecular dynamic studies were employed to suggest the adsorption mechanism.

Keywords: *Argania spinosa*; chemical composition; corrosion; mild steel; antioxidant activity; molecular dynamic simulation

1. Introduction

Argan oil is traditionally extracted from kernels of the most remarkable species in North Africa: the argan tree (*Argania spinosa*). The botanical and bio-ecological interests, as well as the social value of this tree, make it an endemic tree in Morocco [1]. Many studies were initiated and published seeking to prove or deny the knowledge of traditional medicine in the Arabic world. Besides human nutrition, AO was used for cosmetics and to treat some diseases such as: diabetes [2], malaria [3], rheumatisms, lung infections, newborn gastrointestinal disorders [4], atherosclerosis, and hypercholesterolemia [5].

Thanks to its various mechanical proprieties, mild steel is widely used in the industrial field. By 2019, the world total steel production was estimated to be 1.9625 billion tonnes and in 2020, the United Kingdom economy gained GBP 2.0 billion in terms of gross value added (GVA) [6]. These statistics show the importance of mild steel in human lives. However, iron alloys in general are not stable and exhibit lower corrosion resistance than other aluminum and copper alloys [6,7]. According to a benchmark study released in 2002 by the US Federal Highway Administration (FHWA), this natural process, corrosion, represents 3.1% of the annual US gross domestic product (GDP) [8]. Among the solutions provided to solve this problem or at least decreases its damages we find the use of plant extracts to be eco-friendly corrosion inhibitors [9]. Different plant parts, such as roots, seeds, flowers, barks, leaves, and fruits, were used to extract potential corrosion inhibitors either by maceration and Soxhlet (for extraction by organic solvents) or hydro-distillation (for essential oils extraction). These extracts were tested as corrosion inhibitors for mild steel in acidic media and showed remarkable inhibition efficiencies [10–16]. The use of these plant parts as corrosion inhibitors is an added value to the plant and a chance to valorize it when it could be an invasive species and locals are having a hard time to stop it spread in nature.

Several studies showed that the chemical composition of argan oil depends not only on the extraction method used but also on the origin of kernels (climatic conditions of the area) and the storage condition [17]. Since the chemical composition is related to the origin of the kernel, this work aims to present the chemical composition of argan oil (AO) and the hexanic extract of roasted almonds (HERA) from a small village, Lagfifate in Taroudant, in order to provide data that can be compared with other results from other places. This work also aims to evaluate, experimentally and theoretically, the antioxidant and corrosion inhibition effects of two extracts from *Argania spinosa*'s almonds.

2. Materials and Methods

2.1. Samples

The alimentary argan oil was prepared traditionally in February 2018 following the steps clearly described by Mechqoq et al. [17]. HERA was obtained using Soxhlet apparatus and hexane as solvent. The seeds used for the preparation of AO and HERA were collected in September 2017 in Lagfifate (Souss-Massa region—Morocco: 30°17′41″ N 9°17′21″ W). Before the extraction, 400 g of argan almonds was carefully roasted and grinded. The traditional extraction of AO is a slow process because it relies totally on the extractor strength. To extract 1 L of AO the whole process "nuts breaking, kernels roasting, grinding and hand pressing" took 10 h. Whereas the preparation of HERA was done by Soxhlet apparatus. The "solvent vaporization-condensation" cycle is repeated for 8 h. It is worthy to mention that the vegetal material was only used for one extraction but the experiment was repeated three times.

The hydrochloric acid used to prepare the aggressive solution was purchased from VWR CHEMICALS co. Whereas, the chemical composition of the mild steel used to conduct this study (in wt%) is 0.21 of C, 0.38 of Si, 0.09 of P, 0.05 of Mn, 0.05 of S, 0.01 of Al and the remainder is iron. For the weight-loss measurements, we used a 2.5 cm × 2.5 cm × 0.3 cm mild steel coupon with the same chemical composition.

2.2. GC-MS Analysis

To identify the chemical composition of AO and HERA, we started by the esterification of their fatty acids, following the standardized NF T60-233 protocol [18]. Briefly, 0.03 g of AO and HERA were dissolved in 4 mL n-hexane, saponified by a 3 mL of 1 M NaOH, and then neutralized with 1 M HCl. The mixture was centrifuged for 5 min and the upper layer containing the fatty acid was collected and esterified by a 30 mL BF_3 solution in excess methanol. Furthermore, 1 µL of AO and HERA methyl esters was injected in a Shimadzu GC system (Kyoto, Japan) equipped with BPX25 capillary column (30 m length, 0.25 mm inner diameter, and 0.25 µm film thickness). The injection was done in a 90:1 split mode and >99% helium gas at a 3 mL/min constant flow rate was used as a carrier gas. The

temperature of the injector, the interface, and the ion source were set at 250 °C while the column oven's temperature was held for 1 min at 50 °C then heated to 250 °C at 10 °C/min. The sample component ionization was done in an (70 eV) EI mode where the mass range scanned from 40 to 300 *m/z*. The identification process of the AO and HERA methyl esters was monitored by LabSolutions (version 2.5, Spain) software and The National Institute of Standards and Technology (NIST) database.

2.3. Weight Loss Measurement

In order to investigate the AO and HERA concentrations' effect on corrosion rate and inhibition efficiency, the previously mentioned specimens were totally immerged in an equal volume of 1 M HCl with or without a defined concentration of AO or HERA, these specimens were abraded with SiC abrasive sheets (180–1200 grade). After 6 h of immersion at 308 K, the inhibition efficiency was calculated using Equation (1):

$$\text{EI } (\%) = \frac{W_{corr}^0 - W_{corr}}{W_{corr}^0} \times 100 \tag{1}$$

W_{corr}^0 and W_{corr} are, respectively, the mild steel weight loss in the absence and the presence of AO or HERA.

Generally, the determination of the weight loss (mg $\times$ cm^{-2} $\times$ h^{-1}) is based on the difference of weight Δm (mg) of the mild steel coupons before and after a fixed time **t** (h) and the global coupons area (cm^2) in touch with the medium. However, the corrosion rate C_R is calculated via Equation (2) and expressed in mm/year allowing the comparison of the results obtained from all over the world.

$$C_R \left(\frac{\text{mm}}{\text{year}} \right) = \frac{87,600 \times W}{D} \tag{2}$$

D is the mild steel density and *W* is the weight loss.

2.4. LANGMUIR Isotherm, Activation and Adsorption Parameters

The same equation (Equation (1)) is used for studying the temperature effect on the corrosion rate, i.e., the inhibition efficiency. During this test, the concentration of AO and HERA was 2 g/L and the immersion time is fixed at 1 h; whereas the temperature was fixed at 308, 318, 328, and 338 K.

Activation energy E_a is a main key to understanding the metal-inhibitor interactions. Comparing the inhibitor and the blank activation energies, Radovici distinguished between two types of metal-inhibitor interactions: an electrostatic ($E_{ai} > E_a$) and a chemical ($E_{ai} < E_a$) interaction [19]. The Arrhenius logarithmic equation (Equation (2)) gives access to the activation energy E_a, while the Arrhenius equation alternative formula (Equation (3)) gives access to other thermodynamic parameters such as adsorption entropy $\Delta S_{ads}{}^0$ and $\Delta H_a{}^0$ adsorption enthalpy.

$$lnC_R = Ln(A) - \frac{E_a}{RT} \tag{3}$$

$$ln \left(\frac{W}{T} \right) = \left(ln \left(\frac{R}{Nh} \right) + \frac{\Delta S_a^0}{R} \right) - \frac{\Delta H_a^0}{RT} \tag{4}$$

where: *A* is a constant, *R* is the gas constant, *N* is the Avogadro's number, and *h* is Planck's constant.

Based on the results of the temperature effect, and in order to define the adsorption thermodynamic parameters, LANGMUIR isotherm was plotted using Equation (4):

$$\frac{C_{inh}}{\theta} = \frac{1}{K_{ads}} + C_{inh} \tag{5}$$

where C_{inh} is the concentration of the tested inhibitor, θ is the area coverage, and K_{ads} is the the adsorption-desorption equilibrium constant [20]. The calculated K_{ads} from Equation (4) allows for the calculation of the free adsorption energy $\Delta G^{\circ}{}_{ads}$ using Equation (6):

$$\Delta G^{\circ}_{ads} = -RT \times ln(K_{ads} \times C_M(solvent)) \tag{6}$$

The $C_M(solvent)$ is the solvent's molar concentration which is equal to 55.5 mol·L^{-1} for H_2O. R is the gas constant (R = 8.314 J·K^{-1}·mol^{-1}).

2.5. EIS and Polarization Curves

Involving the under static condition, a PJZ100 radiometer analytical potentiostat controlled by Tacussel corrosion analysis software model (Voltamaster 4) was employed. A three electrode cell, thermostatically stabilized at 308 K, is used to perform electrochemical tests. The working electrode is a 1 cm^2 disc made from one of the previously mentioned coupons. A saturated calomel electrode SCE was used as reference electrode. With the same surface area as the working electrode, a platinum electrode was used as auxiliary electrode. Seeking to define the open circuit potential E_{OCP}, the working electrode is immersed for 30 min in the test solution to achieve a steady state OCP. At E_{OCP} and a frequency ranged between 100 KHz and 0.1 Hz, the EIS experiments were conducted with 10 points per decade. Nyquist plots were established using this measurement results. Once the EIS was finished and after 5 min of E_{OCP}, the polarization measurement of the tested solutions were scanned from -800 to -200 mV by applying a 1 mV s^{-1} as a scan rate [21].

The inhibition efficiency for EIS and polarization measurements was calculated using, respectively, Equations (7) and (8):

$$E_R\% = \frac{R_{t(inh)} - R_t}{R_{t(inh)}} \times 100 \tag{7}$$

$$E_i\% = \frac{I^0_{corr} - I_{corr}}{I^O_{corr}} \times 100 \tag{8}$$

where $R_{t(inh)}$ and R_t (respectively, I_{corr} and I^0_{corr}) are the charge transfer resistances (respectively, current densities) for the inhibited and uninhibited medium.

Further technical and theoretical details on the electrochemical methods and weight loss measurement were published by our lab members in their works [22–27].

2.6. Antioxidant Activity

2.6.1. DPPH Radical Scavenging Assay

The AO and HERA ability for scavenging the DPPH radical was determined as described by Zimila et al. with minor modifications [28]. Briefly, a serial dilution (8–0.5 mg/mL) of AO and HERA was prepared in methanol while the standard antioxidants' (quercetin and gallic acid) concentrations were 200 to 12.5 µg/mL. Furthermore, 0.2 mL of the methanolic aliquots were added to 1.8 mL DPPH aliquot (4 mg/100 mL of methanol). After 30 min of incubation in the dark at room temperature, the absorbance was recorded at 517 nm against the blank (0.2 mL methanol + 1.8 mL DPPH aliquot) and the inhibition efficiency *IE* (%) was calculated using the following equation:

$$IE(\%) = \frac{A_{blank} - A_{sample/standard}}{A_{blank}} \times 100 \tag{9}$$

where A_{blank} represents the absorbance of the blank and $A_{sample/standard}$ represents the measured absorbance of the sample or the antioxidants standards.

2.6.2. Ferric Reducing Antioxidant Power (FRAP) Assay

The FRAP was measured by relying on the protocol described by Zimila et al. with minor modifications [28]. Briefly, 400 µL of methanol, AO, HERA, and standard antioxi-

dants were mixed with 1.25 mL of 0.2 M phosphate buffer (pH 6.6) and 1.25 mL of 1% *w/v* $K_3Fe(CN)_6$. The tubes were immediately incubated for 20 min at 50 °C and then cooled at room temperature. The mixture was acidified with 1.25 mL of 10% *w/v* trichloroacetic acid and centrifuged for 10 min at 3000 rpm. One milliliter of supernatant was added to an equal volume of distilled water and 0.25 mL of 0.1% *w/v* of $FeCl_3$. The absorbance was measured at 700 nm against the blank containing all reagents and methanol. The concentrations of AO, HERA, and standard antioxidants are the same as those mentioned in DPPH radical scavenging assay. The *FRAP* (%) was calculated using the following equation:

$$FRAP\ (\%) = \frac{A_{blank} - A_{sample/standard}}{A_{blank}} \times 100 \tag{10}$$

where A_{blank} represents the absorbance of the blank and $A_{sample/standard}$ represents the measured absorbance of the sample or the antioxidants standards.

2.7. Computational Study

Density functional theory (DFT) with unrestricted spin using DMol$_3$ as implemented module in Materials Studio software (Accelrys Inc., San Diego, CA, USA) was applied. Generalized gradient approximation (GGA) with the Becke3-Lee-Yang-parr (B3LYP) level using the 6-311G** basis set were applied. The chemical reactivity parameters computed for AO and HERA, are as follows: S—softness (measurement of molecules' stability), η—hardness (reverse of softness), DM—dipolmoment, chemical potential, χ—electronegativity(grabbing-electrons-power), μ− and μ+—electronic affinity transfer and accept, respectively, ω− and ω+—molecule suitability for providing and gaining an electron, respectively, ωi—electrophilicity index (evaluating the relative strengths of electron donors and acceptors), ΔNmax = χ/2η (highest amount of electrons that can be exchanged in a chemical reaction), I—ionization-potential, and A—electron affinity.

2.8. Molecular Dynamic (MD) Simulations

MD can be simulated by the adsorption behavior of AO and HERA inhibitor into the mild steel surface using the Adsorption-Locator-module (Materials studio). Fe (1 0 0) plane with simulation box (22.90 Å × 57.26 Å × 26.68 Å) was applied in the adsorption process simulation. "$E_{adsorbtion}$" interaction energy between Fe and AO and HERA inhibitors was equationally represented as "$E_{adsorbtion} = E_{total} − (E_{Fe} + E_{inhibitor})$", while "$E_{total}$" total energy of crystal combined with inhibitor and E_{inh}; inhibitor energy, E_{Fe}—iron surface energy. COMPASS force field was used to optimize the adsorption system

2.9. Molecular Docking Analysis

The molecular docking profile was utilized over the binding site of human Keap1 (PDB Code: 4L7B) to predict the probable binding mode of the reference inhibitor (quercetin) and AO and HERA as candidate inhibitors. Schrödinger's Protein Preparation Wizard [29] was to handle the *h*Keap1; polar H-atoms were generated, nonpolar H-atoms were removed, and then charges were added. Lamarckian-Genetic-Algorithm offered by AutoDock Vina [30] was used to perform rigid docking, with 25 × 25 × 25 grid map, creating the Keap1-binding-pocket in the cube's center. For evaluation, the best interaction binding energy (kcal mol^{-1}) was chosen to predict the possible binding mode of quercetin and AO and HERA as potential inhibitors.

3. Results and Discussion

3.1. Chemical Composition

The extraction yield of AO and HERA is, respectively, $28 \pm 2\%$ and $55 \pm 1\%$ *w/w*. The high extraction yield of HERA is justified by the extraction mechanism itself: with every extraction cycle using Soxhlet apparatus, the roasted almonds are soaked in fresh hexane. On the other hand, the traditional AO extraction is based on the strength of women's arms. In their published works, Charrouf et al. mentioned the impact of the extraction process

on the extraction yield: the use of hydraulic presses decreased the amount of time needed to extract 1 L of AO by five times and increased the extraction yield from 29 to 50% [31]; while organic solvent extraction gives a yield ranging from 50 to 57% [32].

The results of GC-MS analysis (Figure 1 and Table 1) reveal that linoleic acid (C18:2 n-6) is the predominant fatty acid in AO ($60.55 \pm 0.16\%$) and HERA ($32.26 \pm 0.33\%$). While the second and the third predominant fatty acids for AO are, respectively, stearic acid (C18:0) ($20.24 \pm 0.17\%$) and palmitic acid (C16:0) ($15.87 \pm 0.17\%$); its order is reversed for HERA, i.e., $15.37 \pm 0.41\%$ for palmitic acid and $5.14 \pm 0.12\%$ for stearic acid.
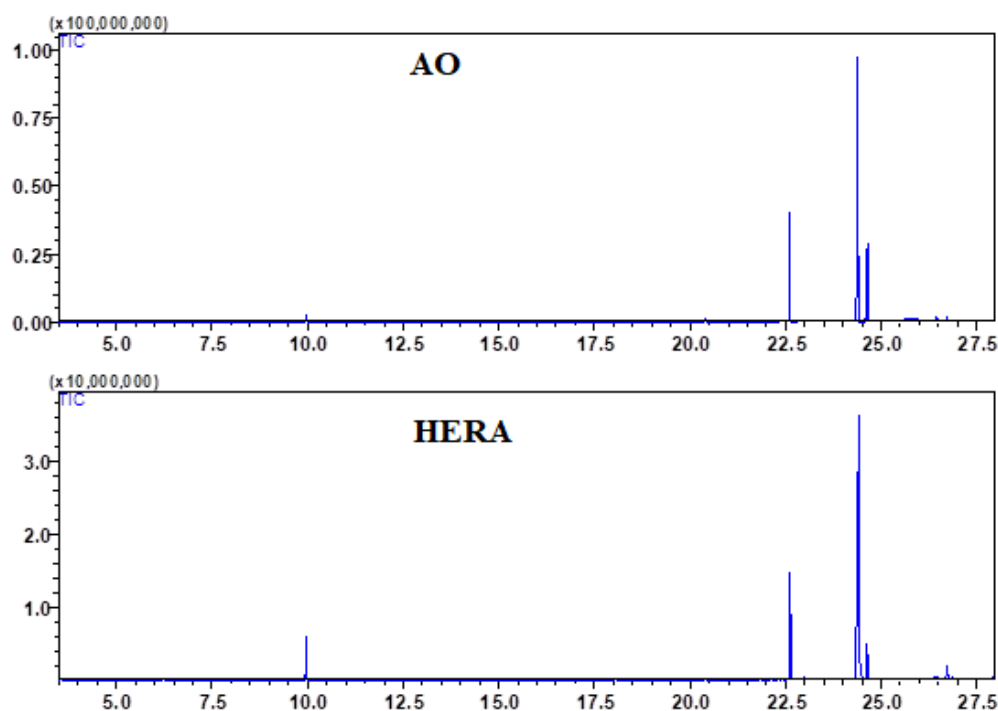

Figure 1. GC-MS chromatogram of AO and HERA.

Table 1. Chemical composition of AO and HERA.

		% (Area Calculations)	
Compd.	RT	AO	HERA
Myristic acid (C14:0)	20.39 ± 0.02	0.69 ± 0.13	0.24 ± 0.07
Palmitoleic acid (C16:1)	22.41 ± 0.03	0.41 ± 0.09	0.15 ± 0.03
Palmitic acid (C16:0)	22.62 ± 0.06	15.87 ± 0.17	**15.37 ± 0.41**
Linoleic acid (C18:2 n-6)	24.38 ± 0.08	**60.55 ± 0.16**	**32.26 ± 0.33**
Stearic acid (C18:0)	24.64 ± 0.05	**20.24 ± 0.17**	5.14 ± 0.12

3.2. Weight Loss Measurements

Table 2 shows the effect of addition of different concentrations of AO and HERA on mild steel corrosion in 1 M HCl. These results show that increasing the tested inhibitor concentration leads to a decrease in corrosion rate, whereas the inhibition efficiency increases. Moreover, the corrosion rate also depends on the molarity of the aggressive media: in our study the C_R is 8.3 mm/year whereas Abhinay Thakur et al. found that C_R of 0.5 M hydrochloric acid is 3.07 mm/year [33]. At the same concentration (2 g/L), AO is more efficient (87%) than HERA (84%). This result could be attributed to the extraction mode, i.e., HERA was extracted using n-hexane (non-polar solvent) which has a great affinity for non-polar molecules. On the other hand, AO may contain polar and non-polar species. The

efficiency of AO could be justified by the positive influence of adding salt to the dough while it has been hand-pressed. This suggestion was proved by Libin Tang et al. [34]. They found out that the presence of chloride ions stabilizes the inhibitor's adsorption on the metal surface and consequently the inhibition efficiency was improved. The same results are illustrated graphically in Figure 2.

Table 2. AO and HERA concentration effect on mild steel corrosion rate and corrosion inhibition efficiency.

	Concentration (g/L)	W (mg·cm^{-2}·h^{-1})	C_R (mm/year)	EI %
Blank	-	0.7436	8.3	-
AO	0.06	0.3061	3.42	59.75
	0.12	0.2619	2.92	65.83
	0.25	0.1758	1.96	76.19
	0.5	0.1443	1.61	81.42
	1	0.11	1.23	85.36
	2	0.0951	1.06	87.18
HERA	0.06	0.2878	3.21	61.22
	0.12	0.2583	2.88	65.09
	0.25	0.2104	2.35	72.37
	0.5	0.177	1.98	76.28
	1	0.138	1.54	81.42
	2	0.1167	1.3	84.64
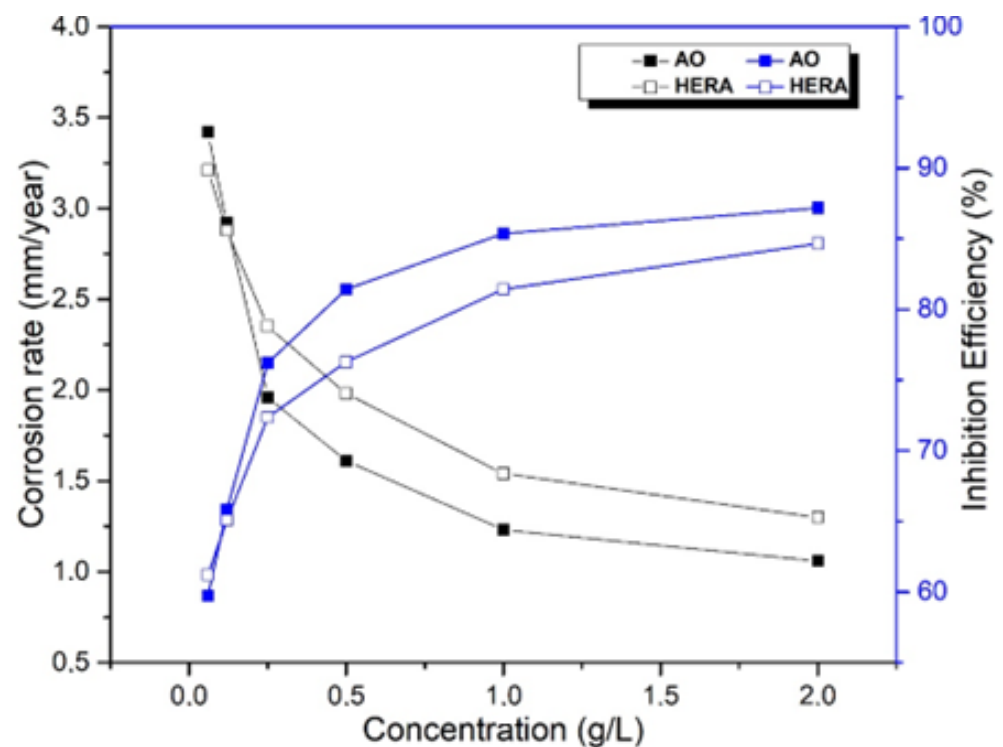
Figure 2. AO and HERA concentration effect on mild steel corrosion rate and corrosion inhibition efficiency.

Even though the gravimetric measurements give an idea about the efficiency of a corrosion inhibitor, it is still incapable of approaching the corrosion mechanisms. For this particular reason scientist use other techniques such as EIS and polarization curves.

3.3. LANGMUIR Isotherm, Activation and Adsorption Parameters

Using the slopes and intercepts of linearly fitted Equations (3) and (4) (Figures 3 and 4), we deduced E_a, ΔS_a^0, and ΔH_a^0 (Table 3).
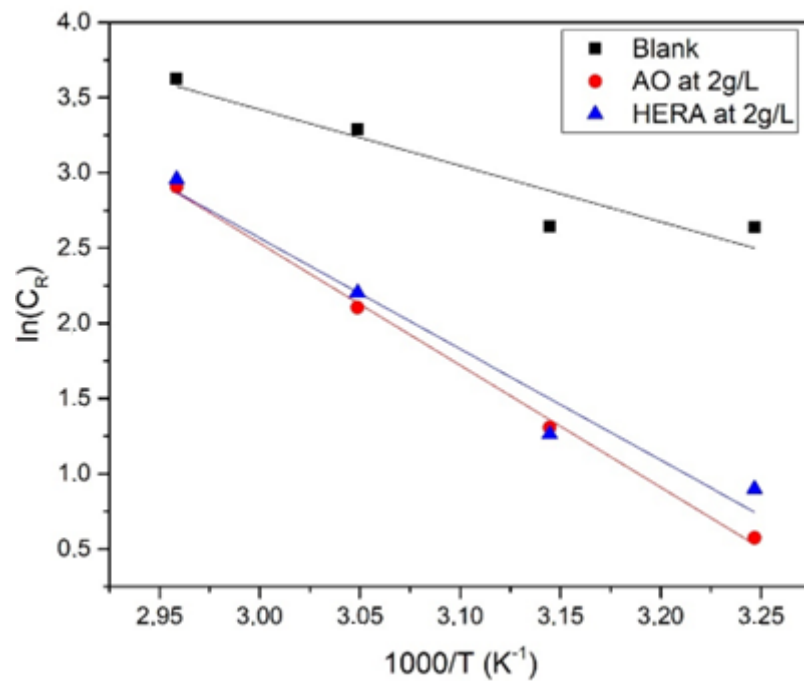
Figure 3. Arrhenius plots for mild steel in 1 M HCl in the absence and the presence of AO and HERA.
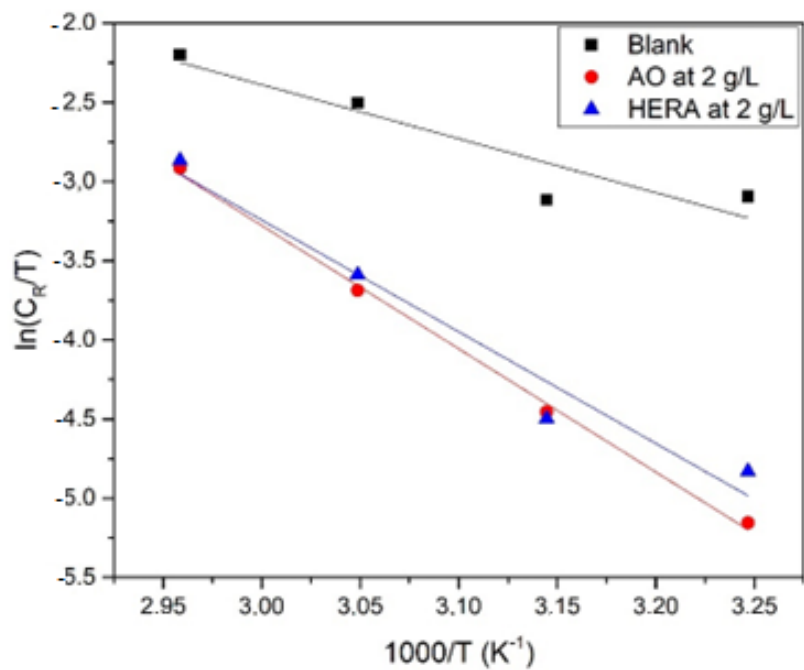
Figure 4. The alternative Arrhenius equation plots for steel in 1 M HCl in the absence and the presence of AO and HERA.

Table 3. Activation parameters in the presence and absence of AO and HERA.

	E_a (KJ·mol^{-1})	ΔH_a^0 (KJ·mol^{-1})	ΔS_a^0 (J·mol^{-1}·K^{-1})	K_{ads}	ΔG_a^0 (KJ·mol^{-1})
Blank	31.031	28.350	−152.415	–	–
AO at 2 g/L	67.407	64.726	−50.682	21.8867×10^4	−31.4871
HERA at 2 g/L	61.343	58.662	−68.586	19.9641×10^4	−31.2516

High ΔH_a^0 values reflect the lowering of the corrosion reaction's energy barrier, i.e., the corrosion reaction is less aggressive when ΔH_a^0 has higher values. The ΔH_a^0 results show that, at 2 g/L, AO is more efficient against mild steel corrosion. In addition, the positive values of ΔH_a^0 reflect the endothermic aspect of the mild steel's slow dissolution process in the inhibited mediums [35]. Negative values of ΔS_a^0 indicate that the inhibitors are more and more attached to the mild steel surface, which decreases the medium disorder. Furthermore, the inhibited medium ΔS_a^0 values are more positive than the blank. This behavior might be justified by water molecules' desorption during the inhibitor's adsorption [36].

The Langmuir isotherms plotted for AO and HERA (Figure 5) showed an R^2 close to the unit (0.9999 for AO and 0.9995 which reflects that the two tested inhibitors' adsorption obeys the Langmuir isotherm. Slopes, intercepts, and K_{ads} are calculated using Equation (4). the positive values of K_{ads} (21.8867 × 10^4 g/L and 19.9641 × 10^4 g/L, respectively, for AO and HERA at 2 g/L) suggest that AO and HERA adsorption on the mild steal surface is possible [37]. The values of ΔG_a^0 reflect the strong interaction between AO and HERA molecules and the mild steel surface. This interaction leads to the establishment of a chemical barrier between H_3O^+(aq) and Cl^- (aq) ions and the mild steel surface [33]. On the other hand, researchers are more and more convinced that the calculation of $\mathbf{\Delta G_a^0}$ values is meaningless since the Langmuir isotherm is based on the adsorption of identical species (with a precisely defined molecular weight) on a homogenous flat surface [38,39]. This result was mentioned in previously published articles studying plant extracts' adsorption on mild steel as eco-friendly corrosion inhibitors [10,40].
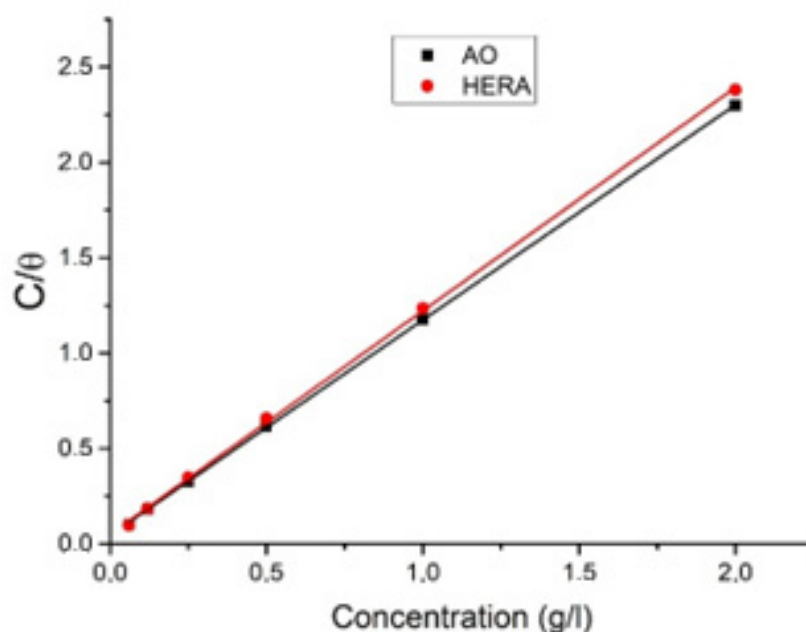
Figure 5. Langmuir adsorption isotherm of mild steel in 1 M HCl in the presence and the absence of AO and HERA.

3.4. Electrochemical Impedance Spectroscopy

In order to understand the action mode of several synthetic and natural corrosion inhibitors on mild steel in acid medium, EIS was exploited in many published studies [41–43]. Regarding the applied potential used in this method, a small sinusoidal excitation is imposed and the electrochemical metal-solution interface results in impedance. Using the different impedance data, Nyquist plots for mild steel in 1 M HCl at 308 K containing different concentrations of AO and HERA (Figure 6) were established. Table 4 includes the impedance parameters derived from the Nyquist plots.

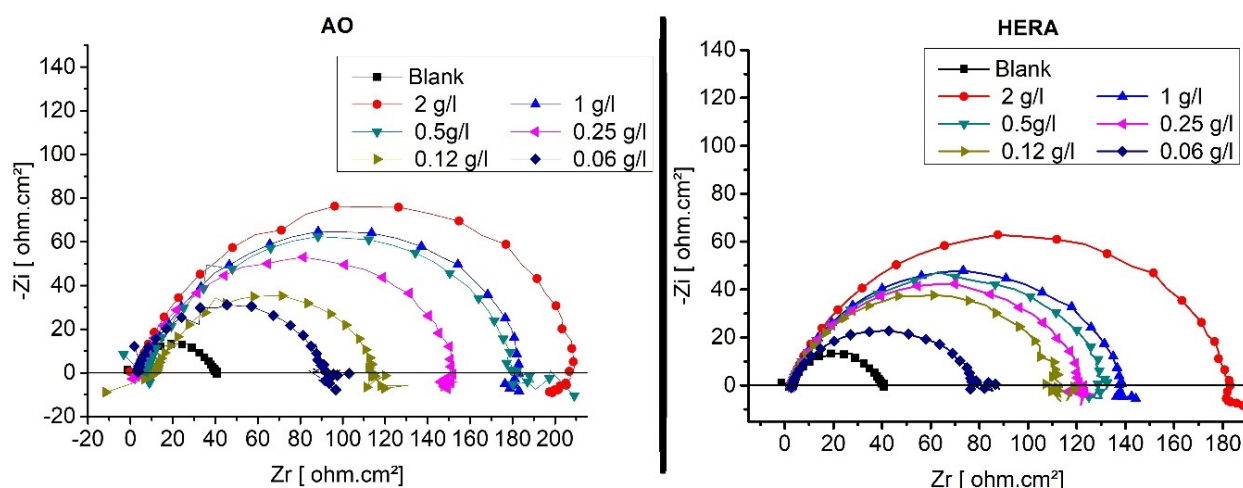**Figure 6.** Nyquist plots for mild steel in 1 M HCl in presence and absence of AO and HERA.

Table 4. EIS parameters of mild steel in 1 M HCl in presence and absence of AO and HERA.

	Concentration (g/L)	R_s ($\Omega \cdot cm^2$)	R_t ($\Omega \cdot cm^2$)	f_{max} (Hz)	C_{dl} ($\mu F/cm^2$)	E (%)
Blank	-	2.63	40.31	29.59	133.41	-
AO	0.06	2.91	92.59	24.21	75.91	56.47
	0.12	9.84	114.7	18.28	72.81	64.86
	0.25	3.68	152.5	15.44	70.99	73.57
	0.5	7.83	182.7	12.01	70.33	77.94
	1	6.19	187.2	12.09	67.68	78.47
	2	3.28	212.3	12.31	60.92	81.01
HERA	0.06	2.75	79.22	14.35	140.07	49.12
	0.12	2.86	112.1	15.42	92.08	64.04
	0.25	2.80	122.9	19.55	77.72	67.20
	0.5	2.85	132.3	15.48	74.15	69.53
	1	2.97	138.6	15.28	66.24	70.92
	2	3.04	182.7	15.55	56.05	77.94

The difference in impedance at lower and higher frequencies allows the calculation of charge transfer resistances [44]. At the imaginary component's maximum Nyquist plot, double layer capacitances (C_{dl}) were calculated by use of Equation (10):

$$C_{dl} = \frac{1}{2\pi \times f_{max} \times R_t} \tag{11}$$

where R_t is the charge transfer resistance ($\Omega \cdot cm^2$), f_{max} is the maximum frequency (Hz), and C_{dl} is double layer capacitance ($\mu F \cdot cm^{-2}$).

The obtained plots were depressed and semi-circular in shape with the center below the impedance's real component. Deviation of perfect circular shape is often related to the frequency dispersion of interfacial impedance which arises because of surface roughness and interfacial phenomena [45]. The plots' sizes and shapes were increased by increasing the inhibitors' concentrations, indicating that the corrosion of mild steel is mainly controlled by a charge transfer process [46]. We notice that an increase in inhibitors' concentrations provokes an increased charge transfer resistances value; whereas, the double-layer values decrease. It has been reported that the adsorption process on the metal surface is characterized by a decrease in double layer values [44]. Charrouf et al. proved that the salt is added to the oil in order to ameliorate its preservation [1]. This study proves that in addition to its preservative role, salt ameliorates corrosion inhibition efficiency: HERA, the tested

inhibitor which does not contain salt shows efficiency ($\approx$78% at 2 g/L) less than AO ($\approx$81% at 2 g/L).

Plotting the log|Z| phase degree versus log frequency allows the presentation of EIS data in a different way: Bode diagrams (Figure 7). The log|Z| values increase as AO and HERA concentrations increase in the frequency range scanned in this study. The frequency range of the maximum phase angle is also expanded. The Bode results of AO and HERA show that the two tested inhibitors offer an acceptable corrosion inhibition for mild steel [33]. As an equivalent circuit we suggest a simple circuit formed by the parallel association of a capacitor (double-layer capacitance) and a resister (charge transfer resistance) connected to another resistor (solution resistance) (Figure 8).
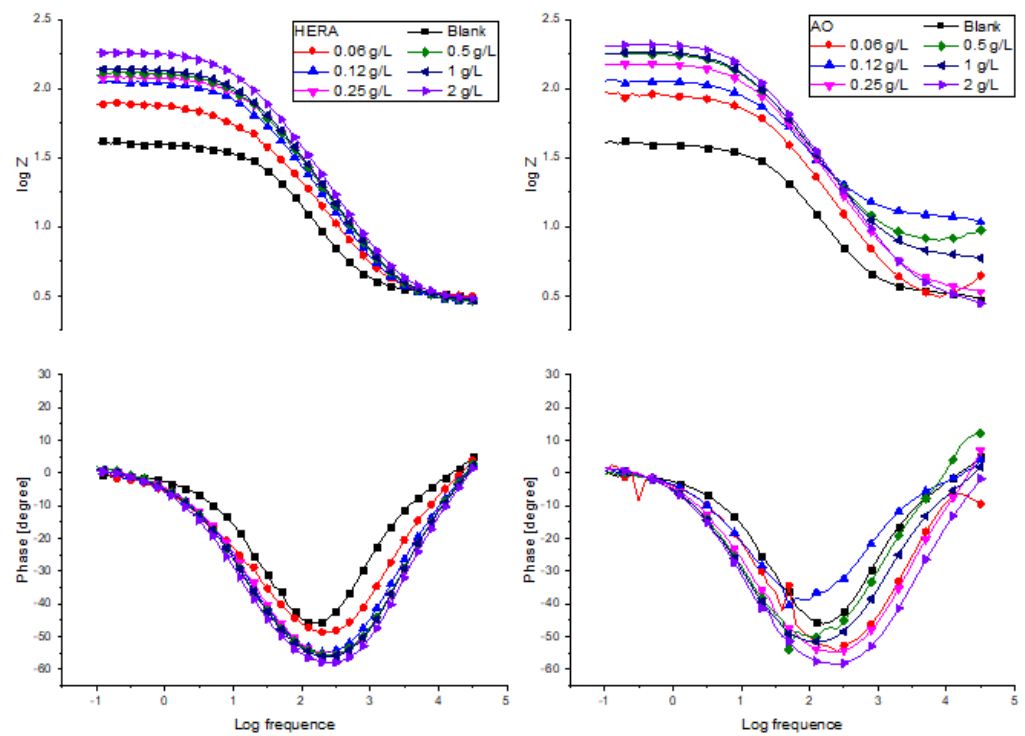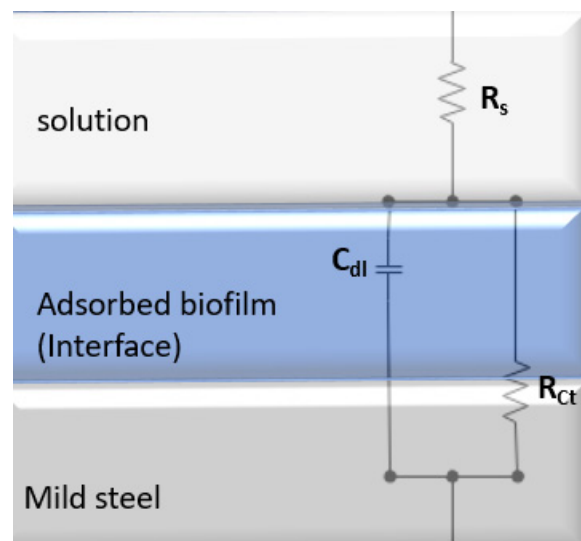

Figure 7. Bode diagrams of AO and HERA.

Figure 8. Suggested equivalent circuit.

3.5. Polarization Curves

Anodic and cathodic polarization curves of mild steel in 1 M HCl medium at various concentrations of tested inhibitors at 308 K are shown in Figure 9. Corrosion data including corrosion potential (E_{corr}), corrosion current densities (I_{corr}), anodic Tafel slope (β_a), cathodic Tafel slope (β_c), and inhibition efficiency are listed in Table 5. The inhibition efficiency ($E_i\%$) was calculated from polarization measurements using Equation (11).

$$E_i\% = \frac{I_{corr}^0 - I_{corr}}{I_{corr}^O} \times 100 \tag{12}$$

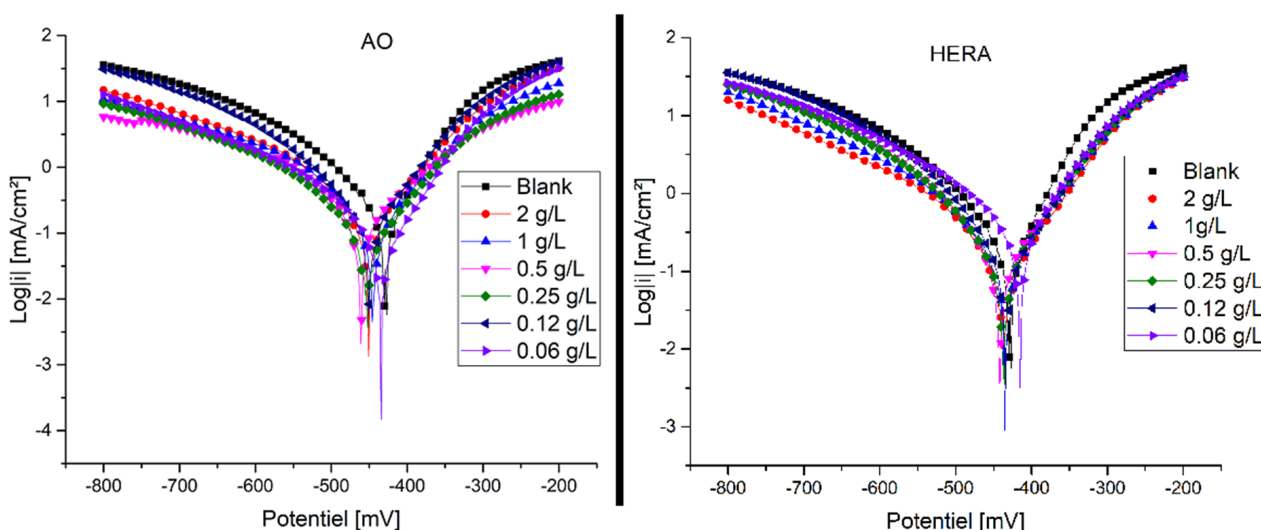where I_{corr} and I_{corr}^0 are, respectively, the inhibited and uninhibited current densities.

Figure 9. Polarization curves of mild steel in 1 M HCl in presence and absence of AO and HERA.

Table 5. Potentiodynamic polarization descriptors of mild steel in 1 M HCl in presence and absence of AO and HERA.

	Concentration (g/L)	E_{corr} (mV)	β_c (mV/Dec)	β_a (mV/Dec)	I_{corr} (mA/cm^2)	E (%)
Blank	-	−454	−182.9	151.8	1.95	-
AO	0.06	−452	−175.6	125.1	0.64	67.07
	0.12	−453.2	−228.9	128.3	0.58	70.60
	0.25	−462.8	−270.1	189	0.55	71.94
	0.5	−447.7	−225.2	134.9	0.47	76.03
	1	−454	−213.2	137.1	0.32	83.44
	2	−436	−189.6	93.5	0.24	**87.88**
HERA	0.06	−416.8	−193.3	102.1	0.55	72.01
	0.12	−437.2	−207	116.1	0.44	77.65
	0.25	−435.7	−138.6	104.9	0.37	80.75
	0.5	−439.2	−204.9	111.9	0.35	82.22
	1	−438.6	−156.5	107.1	0.34	82.52
	2	−443.3	−147.9	109.1	0.33	**82.91**

Analyzing Figure 9 and Table 5, we saw a shift in the anodic and cathodic curves towards low current densities, which indicates that the two processes of hydrogen ion reduction and mild steel anodic dissolution are limited in the inhibited media [47]. The limitation of these two processes became more intense while AO and HERA concentrations increased. The inhibition efficiency of AO (87.878%) is greater than HERA's efficiency (82.913%). This outcome is entirely in line with our expectations. We assumed that when

using salt during the artisanal extraction of argan oil, that AO may result in an increase in chloride ions in the oil. These ions can be adsorbed on the mild steel surface, providing a protective coating and lowering corrosion rates. This result could potentially be owing to the presence of a complex mixture of organic compounds other than fatty acids, that the hexane used for extracting HERA could not dissolve and extract from the argan kernels. In their work on diaminonaphthalene as a mild steel corrosion inhibitor, A. El Guerraf et al. proved the synergetic effect of chloride ions [48]. On the other hand, this finding was further supported by relatively more shifts in the values of βc as compared to the values of β_a. Inspection of Figure 5 reveals that potentiodynamic polarization curves are parallel and similar in the absence and presence of different concentrations of the studied inhibitors indicating that these molecules inhibit metallic corrosion by blocking the active sites present over the metallic surface without changing the mechanism of mild steel corrosion [49].

3.6. Antioxidant Activity

AO and HERA antioxidant activity was assessed by two complementary methods: DPPH radical scavenging assay and ferric reducing antioxidant power (FRAP) assay and was compared to two standard antioxidants (quercetin and gallic acid). Results of measurements performed in triplicate are illustrated using the EC_{50} (Table 6).

Table 6. The DPPH and FRAP EC_{50} values of AO, HERA, quercetin, and gallic acid.

	EC_{50} (μg/mL)	
	DPPH* assay	FRAP assay
AO	3559.08 ± 161.75	1288.58 ± 169.21
HERA	3621.43 ± 316.05	1655.86 ± 240.18
Quercetin	38.62 ± 2.77	20.18 ± 2.23
Gallic Acid	17.41 ± 2.15	17.01 ± 1.35

Even though AO seems to be more efficient as an antioxidant than HERA, their EC_{50} values are much higher than those of standard antioxidants in all methods. The antioxidant properties of numerous essential oils have been related to the predominant fatty acids found in AO and HERA [50–53].

3.7. Theoretical Assay

DFT theory using B3LYP/6-311G** is used for computational study of five of the fatty acids which are extracted from AO and HERA. Figure 10 shows the optimized HOMO, LUMO, and MEPs for the tested compounds. The chemical parameters were calculated using equations as reported by [54], and are listed in Table 7.

3.7.1. Stability Inter- and Intermolecular Interaction against Fe Surface "FMOs" Frontier Molecular Orbitals Analysis

The "HOMO; High occupied molecular orbital" and "LUMO; Low unoccupied molecular orbital" are known as "FMOs; Frontier Molecular orbitals", which are defined by donating/accepting-electrons, respectively, that may determine the path binding of AO and HERA with a steel surface [55]. The FMO gap is used to measure a molecule's chemical reactivity and kinetic stability. Raising the inhibitor's HOMO energy and reducing the surface's LUMO energy, improved (inhibitor-surface) stabilization [56].

E_{HOMO} in aqueous phase is higher than gas phase and the components are arranged in decreasing order as follows: **Palmitic acid > Palmitoleic > Myristic acid > Stearic > Linoleic acid** (Table 7). The greater the E_{HOMO} value is than E_{LUMO}, the greater the likelihood of losing valance electrons and the greater the tendency to donate electrons toward the surface of iron, and greater inhibition potency than the gas phase [56,57]. The **HOMOs** were localized over all carboxy groups in all tested fatty acids while **LUMOs** were tagged

over the aliphatic group (Figure 10). The negative E_{HOMOs} and E_{LUMOs} indicated that the charge was able to migrate from AO and HERA to the Fe surface, which penetrated via the carboxylic centers.

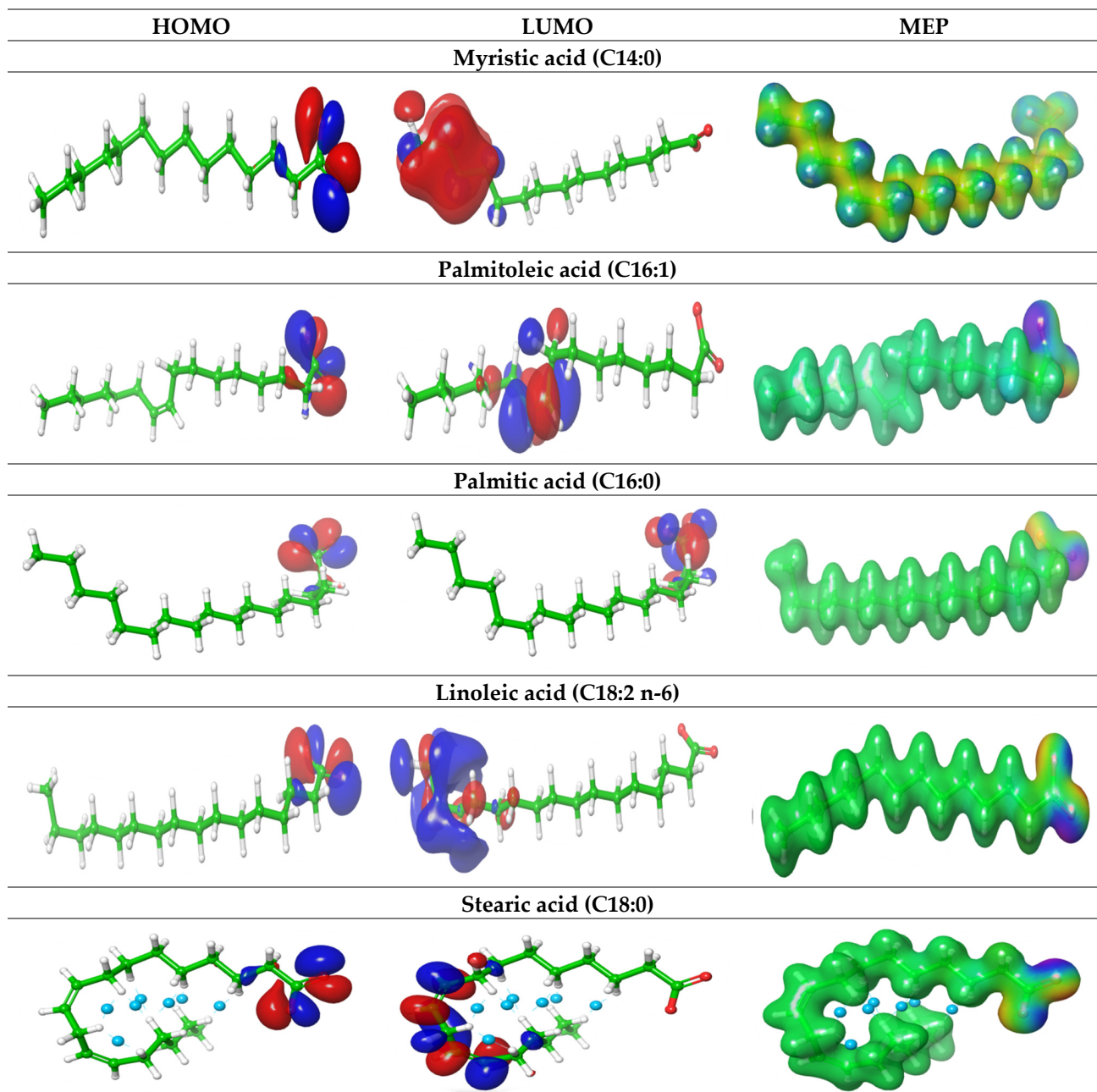| HOMO	LUMO	MEP
Myristic acid (C14:0)		
Palmitoleic acid (C16:1)		
Palmitic acid (C16:0)		
Linoleic acid (C18:2 n-6)		
Stearic acid (C18:0)		

Figure 10. FMOs obtained by DFT/B3YLB/6-311G** for AO and HERA.

"ESP" Molecular-Electrostatic-Potential Profile

In the adsorption process, "ESP; molecular-electrostatic-potential" for the AO and HERA inhibitors is able to identify Fe adsorption sites [58], by finding the balance between scattering and attractive interactions. The scattering force (nuclei with "+" charge) signified with blue color caused electron-donation-power.

The attractive force with "-" charge, associated with electron accepting and expressed as orange, yellow, and red. The green color represents intermediate potential value. ESP was graphically depicted for AO and HERA in Figure 10. The negative charges were allocated as follows: **Myristic acid > Palmitic acid > Stearic acid> Linoleic > Palmitoleic**

acid. ESP surfaces' color variation showed the variation for their values. Highest negative region related to the highest efficiency for their penetration effect over the Fe surface.

Table 7. Calculated reactivity parameters in electron volts except dipole moment in debye for AO and HERA at DFT/B3YLB/6-311G**.

	HOMO	LUMO	ΔG	DM	η	S	χ	I	A	EP	ωi	μ+	μ−	ω−	ω+	ΔEBD	ΔNmax
						(Gas phase)											
Myristic acid (C14:0)	−1.90	−3.54	1.63	36.37	1.63	438.65	1.63	−0.27	−3.54	−1.90	0.82	2.72	1.09	0.27	0.82	−0.54	−14.97
Palmitoleic acid (C16:1)	−1.63	−4.35	−2.72	32.07	1.09	685.45	1.09	−0.27	−2.45	−1.36	0.54	1.90	0.82	0.27	0.54	−0.27	−15.78
Palmitic acid (C16:0)	−2.18	−3.27	−1.09	35.13	1.63	449.26	1.63	−0.27	−3.54	−1.90	0.82	2.72	1.09	0.27	0.82	−0.54	−15.51
Linoleic acid (C18:2 n-6)	−2.45	−3.54	−1.09	33.21	1.63	427.49	1.63	−0.27	−3.81	−1.90	0.82	2.72	1.09	0.27	0.82	−0.54	−15.51
Stearic acid (C18:0)	−1.66	−4.90	−3.24	24.58	0.82	777.70	0.82	−0.27	−2.18	−1.09	0.54	1.63	0.54	0.27	0.54	−0.27	−16.05
						(Aqueous Phase)											
Myristic acid (C14:0)	−6.26	−1.90	4.35	39.16	4.08	181.77	4.08	6.26	−1.90	2.18	0.00	−0.27	−4.08	2.18	0.00	−1.09	−7.62
Palmitoleic acid (C16:1)	−6.80	−0.54	6.26	39.16	3.54	217.42	3.54	6.26	−0.54	2.72	0.82	−1.09	−4.63	2.99	0.82	−0.82	−11.16
Palmitic acid (C16:0)	−7.35	−1.36	5.99	38.69	4.35	184.49	4.08	6.26	−1.90	2.18	0.00	−0.27	−4.08	2.18	0.00	−1.09	−7.62
Linoleic acid (C18:2 n-6)	−5.71	−1.63	4.08	37.09	4.63	185.31	4.08	6.26	−1.90	2.18	0.00	−0.27	−4.08	2.18	0.00	−1.09	−7.62
Stearic acid (C18:0)	−7.62	−0.27	7.35	28.38	3.27	228.30	3.27	6.26	−0.27	2.99	1.09	−1.36	−4.63	3.27	1.09	−0.82	−12.52

S—softness (measurement of molecules' stability), η—hardness (reverse of softness), DM—dipolmoment, χ—electronegativity(grabbing-electrons-power), μ− and μ+—electronic affinity transfer and accept, respectively, ω− and ω+—molecule suitability for provide and gain an electron respectively, ωi—electrophilicity index (evaluating the relative strengths of electron donors and acceptors), $\Delta Nmax = \chi/2\eta$ (highest amount of electrons that can be exchanged in a chemical reaction), I—ionization-potential, A—electron affinity.

3.7.2. Global Chemical Reactivity

The interaction between $HOMO_{inhibitor}$ and $LUMO_{surface}$ has indirectly stabilized with energy gap "**ΔG**". The stability index for AO and HERA adhering to Fe surfaces was determined by **ΔG**. AO and HERA exhibited lower **ΔG** values in gas phase than liquid phase, respectively. These values showed promising reactivity liquid phase (Table 4). Furthermore, **ΔG** related linearly with the soft-nucleophile and hard-electrophile. Thus, the molecule which has a low **ΔG** displayed promising softness "*S*" properties, which leads to being a good inhibitor in acidic media [59–61]. The data obtained from Table 7 demonstrated greater softness values in liquid phase than gas phase.

Furthermore, we examined the amount of electron transfer from the inhibitor (donor) to the Fe (acceptor) by calculating the "μ− & ω−" [59,62]. The inhibition action increases with increasing values for "μ− & ω−", which refers to high ability for donating electron by the inhibitor, respectively, and vice versa for "μ+ & ω+". The liquid phase exhibited higher capacity for sharing electrons than the gas phase. Besides, the highest electrons amount transferred (ΔNmax) for liquid phase (0.055 to 0.059) is more than for the gas phase (−0.28 to −0.46), which supported the claimed experimental findings regarding high efficiency for AO and HERA in liquid phase.

The process of the electron contribution as "Fe → inhibitor" is recognized as energy back-donation, "ΔE_{BD}", which determined the "Inhibitor-Fe$_{surface}$" interaction. The higher ΔE_{BD} in the liquid phase than the gas phase, displayed promising penetration ability with higher inhibition efficiency for liquid phase. The negative values of "ΔE_{BD}, μ+, ω+" proposed that the "Fe → inhibitor" electron follows in liquid phase are more favorable energy than gas phase (Table 7). These findings were consistent with the experimental data.

3.7.3. Molecular Dynamic (MD) Profile

"MD" simulation was performed to provide a better understanding of the "Inhibitor-Fe" interaction (Figure 11). The "Adsorption Locator Model" was utilized to recognize the ideal adsorption site for the mild steel surface against AO and HERA inhibitors. Thus, the lowest inhibition energy is listed in Table 8 as follows: total energy for the substrate, rigid adsorption energy (unrelaxed AO and HERA components which adsorbed on Fe metal), adsorption energy (rigid adsorption and deformation energies), and (d_{Ead}/d_{Ni}) (Fe and AO and HERA inhibitors energy; where one of the inhibitors was removed), binding energy (the negative value of adsorption energy).

Myristic acid (C14:0)
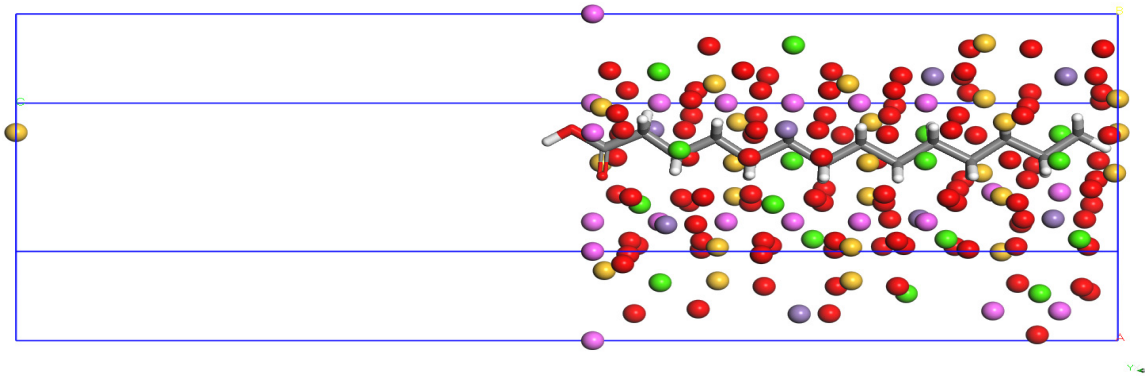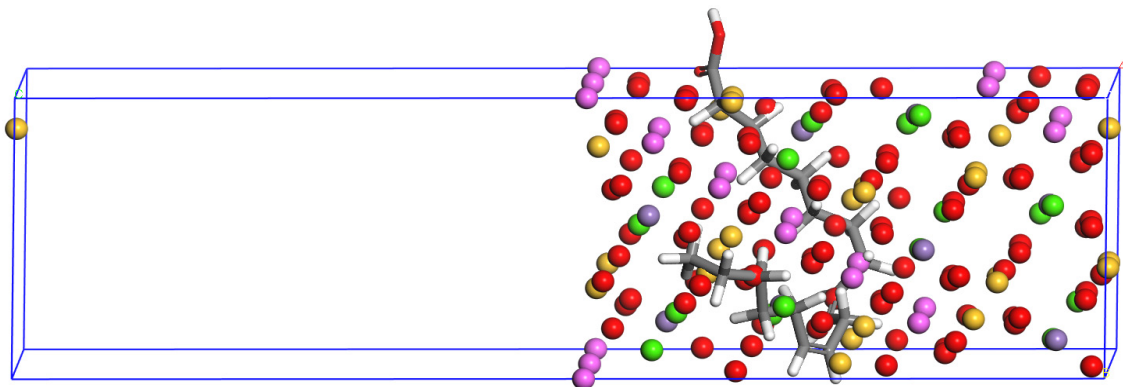

Palmitoleic acid (C16:1)
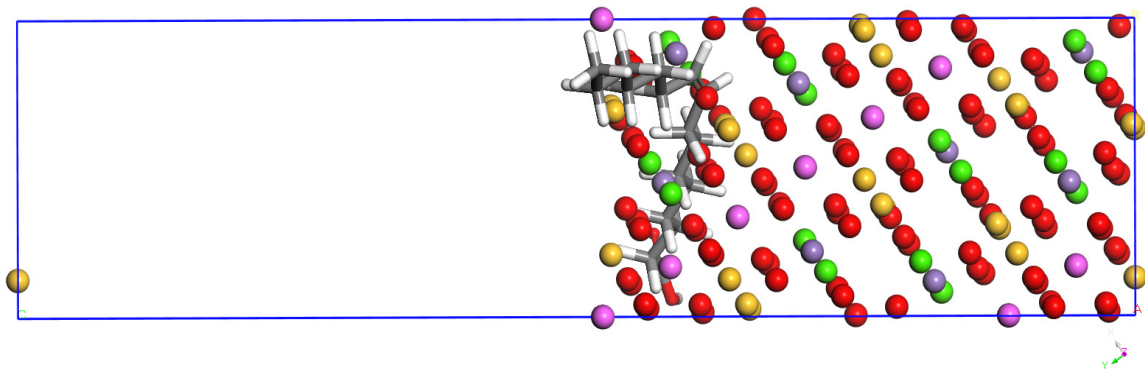
Palmitic acid (C16:0)

Figure 11. *Cont.*

Linoleic acid (C18:2 n-6)
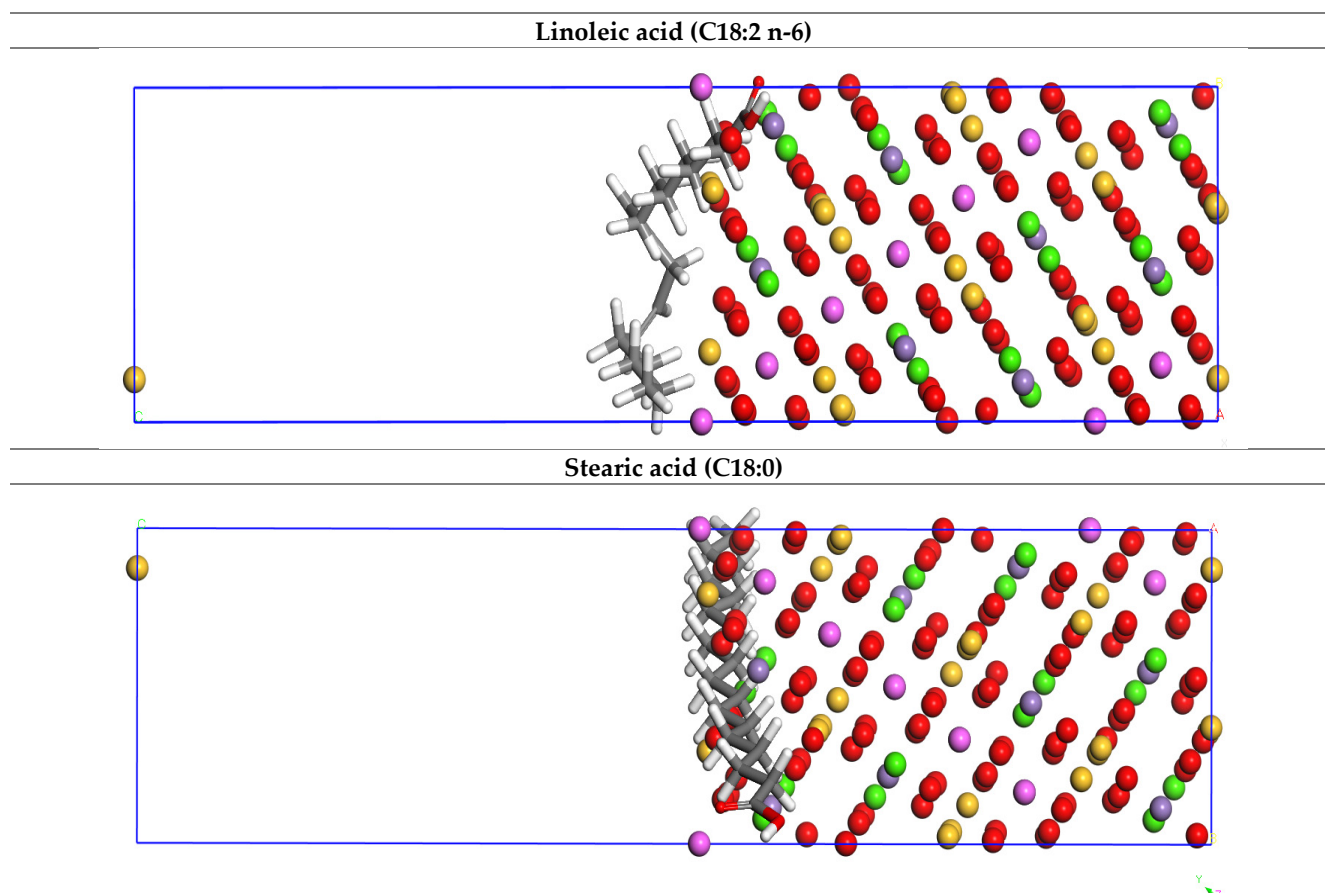

Stearic acid (C18:0)

Figure 11. Side view of molecular simulations for the most favorable modes of adsorption for the inhibitors on Fe (1 0 0) surface.

Table 8. The calculated descriptors (kcal/mol) of AO and HERA on Fe (1 0 0).

Inhibitor Energy	Myristic Acid (C14:0)	Palmitoleic Acid (C16:1)	Palmitic Acid (C16:0)	Linoleic Acid (C18:2 n-6)	Stearic Acid (C18:0)
Total energy	−25.02	−19.70	−25.02	−18.40	−33.12
Adsorption energy	−3.50	−4.178	−4.50	−5.17	−4.99
Rigid adsorption energy	−37.70	−35.64	−71.01	−40.14	−49.68
d_{Ead}/d_{Ni}	−4.50	−5.17	−6.17	−6.17	−5.99

In the stable configuration (Figure 11), palmitoleic, linolenic, and stearic acids were stabilized in parallel to the mild steel surface (1 0 0) plane, while myristic and palmitic acids arranged in plane to the mild steel (1 0 0). In addition, the adsorption energy arranged as **Linoleic > Stearic > Palmitic> Palmitoleic > Myristic** acids (Table 8). This theoretical vision is in line with the experimental findings. The located electron lone pair over O atoms of AO and HERA inhibitors caused a high stability for coordination interaction (inhibitor → Fe). From Figure 11, we can observe that AO and HERA inhibitors are able to adsorb into the mild-steel by the carboxyl groups of AO and HERA inhibitors. Thus, this will cause a mild steel surface to not interact with the acid solution.

3.7.4. Molecular Docking Analysis

We used molecular docking to identify the possible binding mode between the "Keap1-kelch" domain and AO and HERA and compared with quercetin, which acts as reference inhibitor and thus a better indirect antioxidant. A 3D interaction map was created (Figure 12)

which depicts the coupling manner of quercetin at the hKeap1 binding location, (PDB: 4L7B) [61,63] which concluded "Gly364, Leu365, Ala366, Gly367, Arg415, Ile416, Gly417, Val418, Gly462, Gly464, Val465, Gly509, Gly509, Ala510, Gly511, Val512, Ala556, Ala556, Leu557, Gly558, Ile559, Gly603, Gly605, and Val606 residues".
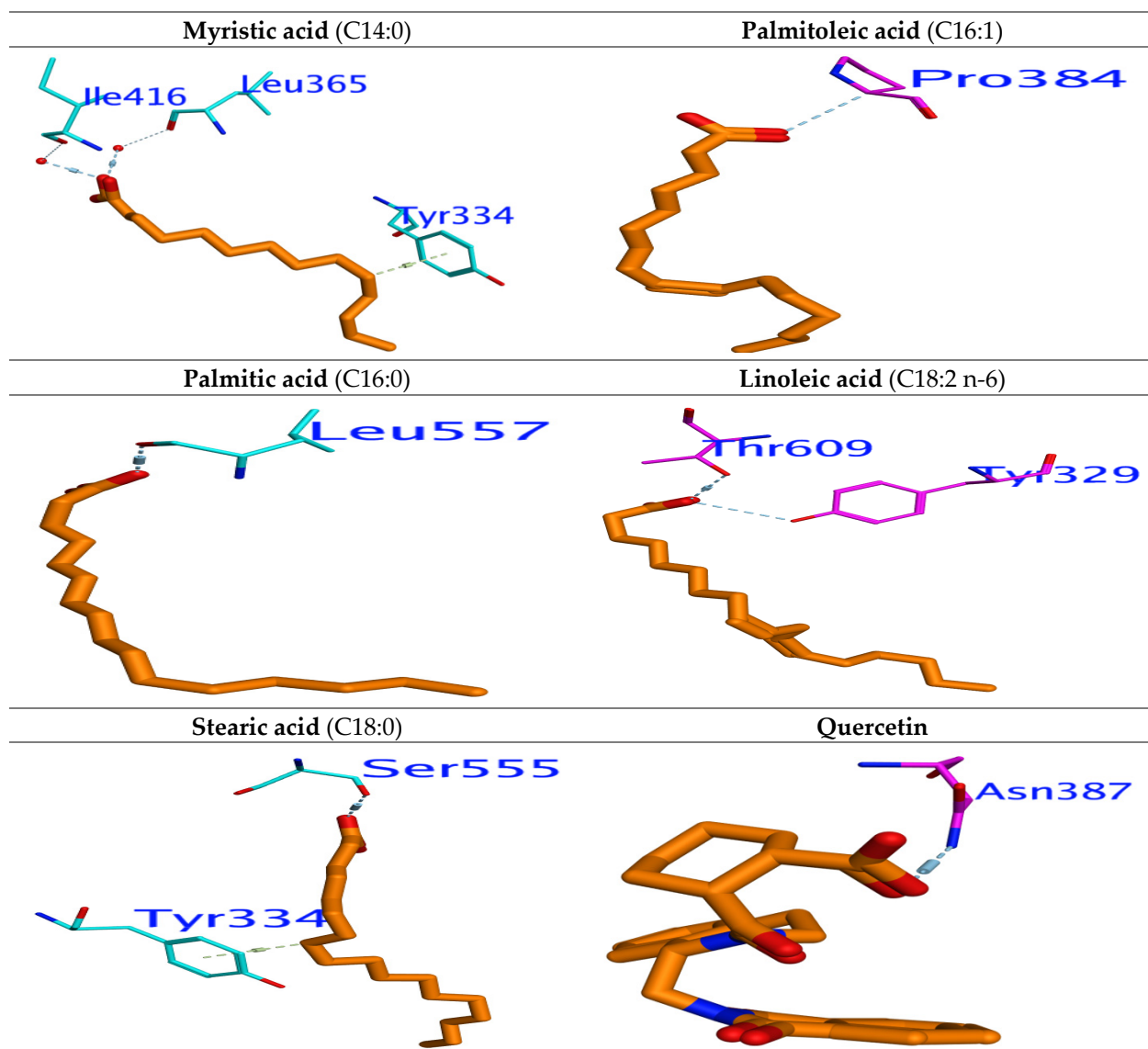

Figure 12. Docking of AO and HERA into (PDB code: 4L7B). H-Bond is characterized by blue lines, hydrophobic interactions are presented by green dotted lines.

The myristic acid has strong hydrogen-bonding interactions with Tyr334. Palmitoleic acid interacted with Pro348 through formation of an H-bond with C=O of carboxylic acid. Besides, OH of the carboxy group for palmitic acid interacted with Leu557 by H-bond doner. Linoleic acid localized in a binding pocket by formation of H-bonds between their C=O with Thr609 and Tyr329. Furthermore, stearic acid interacted with TyrSer55 and Tyr334 (Figure 12).

4. Conclusions

The results obtained at the end of this study prove that the first step of valorization of a plant extract, extraction, is a very important step. The analysis of the chemical composition of both extracts proves that small changes in the extraction protocol led to changes either in

the nature of the chemical compounds existing in the extract or in their amounts. These changes contribute to the development of the antioxidant and the mild steel corrosion prevention abilities of the extract. The weight loss measurements prove that the corrosion's inhibition efficiency, i.e., the corrosion rate is a temperature-related variable and that both extract AO and HERA are a mixed type corrosion inhibitor that controls corrosion inhibition by a charge transfer process. Furthermore, AO showed higher antioxidant activity and mild steel corrosion inhibition ability than HERA illustrating the positive effect of chloride ions present in the AO. These experimental results were supported by quantum simulation performed using (DFT) calculation and molecular dynamics prediction.

Author Contributions: Conceptualization, H.L., O.M. and A.A.; methodology, H.L. and M.E.A.; software, H.L. and A.A.E.; validation, H.E., C.B., R.A.S. and I.R.; formal analysis, H.L.; investigation, H.L. and H.E.; resources, B.H. (Baraa Hafez), B.H. (Belkheir Hammouti) and T.B.H.; data curation, B.H. (Baraa Hafez), B.H. (Belkheir Hammouti) and M.Y.S.; writing—original draft preparation, H.L. and A.A.E.; writing—review and editing, H.L., H.E. and M.M.K.; visualization, S.A.A.; supervision, A.A. and O.M.; project administration, A.A.; funding acquisition, A.A. All authors have read and agreed to the published version of the manuscript.

Institutional Review Board Statement: Not applicable.

Informed Consent Statement: Not applicable.

Data Availability Statement: All data are integrated in this manuscript.

Conflicts of Interest: The authors declare no conflict of interest.

References

1. Charrouf, Z.; Guillaume, D. Ethnoeconomical, ethnomedical, and phytochemical study of *Argania spinosa* (L.) Skeels. *J. Ethnopharmacol.* **1999**, *67*, 7–14. [CrossRef] [PubMed]
2. Bnouham, M.; Bellahcen, S.; Benalla, W.; Legssyer, A.; Ziyyat, A.; Mekhfi, H. Antidiabetic activity assessment of *Argania spinosa* oil. *J. Complement. Integr. Med.* **2008**, *5*. [CrossRef]
3. El Babili, F.; Bouajila, J.; Fouraste, I.; Valentin, A.; Mauret, S.; Moulis, C. Chemical study, antimalarial and antioxidant activities, and cytotoxicity to human breast cancer cells (MCF7) of *Argania spinosa*. *Phytomedicine* **2010**, *17*, 157–160. [CrossRef] [PubMed]
4. Moukal, A. L'arganier, *Argania spinosa* L.(skeels), usage thérapeutique, cosmétique et alimentaire. *Phytothérapie* **2004**, *2*, 135–141. [CrossRef]
5. Berrougui, H.; Ettaib, A.; Gonzalez, M.H.; de Sotomayor, M.A.; Bennani-Kabchi, N.; Hmamouchi, M. Hypolipidemic and hypocholesterolemic effect of argan oil (*Argania spinosa* L.) in Meriones shawi rats. *J. Ethnopharmacol.* **2003**, *89*, 15–18. [CrossRef] [PubMed]
6. Popoola, A.; Olorunniwo, O.; Ige, O. Corrosion resistance through the application of anti-corrosion coatings. *Dev. Corros. Prot.* **2014**, *13*, 241–270.
7. Ziouche, A.; Hammouda, A.; Boucherou, N.; Mokhtari, M.; Hafez, B.; Elmsellem, H.; Abaidia, S. Corrosion Protection Enhancement on Aluminum Alloy And Magnesium Alloy by Mo-CeO2 conversion coating. *Moroc. J. Chem.* **2021**, *9*, 386–393.
8. Jacobson, G.A. NACE International's IMPACT Study Breaks New Ground in Corrosion Management Research and Practice. *Bridge* **2016**, *46*, 30–38.
9. Zakeri, A.; Bahmani, E.; Aghdam, A.S.R. Plant extracts as sustainable and green corrosion inhibitors for protection of ferrous metals in corrosive media: A mini review. *Corros. Commun.* **2022**, *5*, 25–38. [CrossRef]
10. El Azzouzi, M.; Azzaoui, K.; Warad, I.; Hammouti, B.; Shityakov, S.; Sabbahi, R.; Saoiabi, S.; Youssoufi, M.; Akartasse, N.; Jodeh, S. Moroccan, Mauritania, and senegalese gum Arabic variants as green corrosion inhibitors for mild steel in HCl: Weight loss, electrochemical, AFM and XPS studies. *J. Mol. Liq.* **2022**, *347*, 118354. [CrossRef]
11. Arrousse, N.; Mabrouk, E.; Salim, R.; El Hajjaji, F.; Rais, Z.; Taleb, M.; Hammouti, B. Fluorescein as commercial and environmentally friendly inhibitor against corrosion of mild steel in molar hydrochloric acid medium. *Mater. Today Proc.* **2020**, *27*, 3184–3192. [CrossRef]
12. Berrissoul, A.; Ouarhach, A.; Benhiba, F.; Romane, A.; Guenbour, A.; Outada, H.; Dafali, A.; Zarrouk, A. Exploitation of a new green inhibitor against mild steel corrosion in HCl: Experimental, DFT and MD simulation approach. *J. Mol. Liq.* **2022**, *349*, 118102. [CrossRef]

13. Hamdani, I.; Chikri, M.; Fethi, F.; Salhi, A.; Bouyanzer, A.; Zarrouk, A.; Hammouti, B.; Costa, J.; Desjobert, J. Essential Oil Mentha suaveolens L: Chemical Composition, Anticorrosive Properties on Mild Steel in 0.5 M H$_2$SO$_4$ and Chemometric Approach. *J. Mater. Environ. Sci.* **2017**, *8*, 526–538.

14. Mokhtari, O.; Hamdani, I.; Chetouani, A.; Lahrach, A.; El Halouani, H.; Aouniti, A.; Berrabah, M. Inhibition of steel corrosion in 1M HCl by Jatropha curcas oil. *J. Mater. Environ. Sci.* **2014**, *5*, 310–319.

15. Elmsellem, H.; Ouadi, Y.E.; Mokhtari, M.; Bendaif, H.; Steli, H.; Aouniti, A.; Almehdi, A.M.; Abdel-Rahman, I.; Kusuma, H.S.; Hammouti, B. A natural antioxidant and an environmentally friendly inhibitor of mild steel corrosion: A commercial oil of basil (*Ocimum basilicum* L.). *J. Chem. Technol. Metall.* **2019**, *54*.

16. Laaroussi, H.; Aouniti, A.; Hafez, B.; Mokhtari, O.; Sheikh, R.A.; Hamdani, I.; Rahhou, I.; Loukili, E.H.; Belbachir, C.; Hammouti, B.; et al. Argan leaves aqueous extract's antioxidant activity and mild steel corrosion inhibition ability. *Int. J. Corros. Scale Inhib.* **2022**, *11*, 1539–1556. [CrossRef]

17. Mechqoq, H.; El Yaagoubi, M.; El Hamdaoui, A.; Momchilova, S.; Almeida, J.R.G.d.; Msanda, F.; El Aouad, N. Ethnobotany, phytochemistry and biological properties of Argan tree (*Argania spinosa* (L.) Skeels) (Sapotaceae)—A review. *J. Ethnopharmacol.* **2021**, *281*, 114528. [CrossRef]

18. Loukili, E.; Abrigach, F.; Bouhrim, M.; Bnouham, M.; Fauconnier, M.-L.; Ramdani, M. Chemical composition and physicochemical analysis of Opuntia dillenii extracts grown in Morocco. *J. Chem.* **2021**, *2021*, 8858929. [CrossRef]

19. Radovici, O. *Proceedings of the Second European Symposium on Corrosion Inhibitors, Ferrara, Italy*; U.S. Department of Energy: Ferrara, Italy, 1965; p. 178.

20. Fekkar, G.; Yousfi, F.; Elmsellem, H.; Aiboudi, M.; Ramdani, M.; Abdel-Rahman, I.; Hammouti, B.; Bouyazza, L. Eco-friendly Chamaerops humilis L. fruit extract corrosion inhibitor for mild steel in 1 M HCl. *Int. J. Corros. Scale Inhib.* **2020**, *9*, 446–459. [CrossRef]

21. Filali, M.; El Hadrami, E.; Bentama, A.; Hafez, B.; Abdel-Rahman, I.; Harrach, A.; Elmsellem, H.; Hammouti, B.; Mokhtari, M.; Stiriba, S. 3, 6-Di (pyridin-2-yl) pyridazine derivatives as original and new corrosion inhibitors in support of mild steel: Experimental studies and DFT investigational. *Int. J. Corros. Scale Inhib.* **2019**, *8*, 93–109.

22. Benabdellah, M.; Yahyi, A.; Dafali, A.; Aouniti, A.; Hammouti, B.; Ettouhami, A. Corrosion inhibition of steel in molar HCl by triphenyltin2–thiophene carboxylate. *Arab. J. Chem.* **2011**, *4*, 243–247. [CrossRef]

23. Herrag, L.; Hammouti, B.; Elkadiri, S.; Aouniti, A.; Jama, C.; Vezin, H.; Bentiss, F. Adsorption properties and inhibition of mild steel corrosion in hydrochloric solution by some newly synthesized diamine derivatives: Experimental and theoretical investigations. *Corros. Sci.* **2010**, *52*, 3042–3051. [CrossRef]

24. Radi, A.; El Mahi, B.; Aouniti, A.; El Massoudi, M.; Radi, S.; Kaddouri, M.; Chelfi, T.; Jmiai, A.; El Asri, A.; Hammouti, B. Mitigation effect of novel bipyrazole ligand and its copper complex on the corrosion behavior of steel in HCl: Combined experimental and computational studies. *Chem. Phys. Lett.* **2022**, *795*, 139532. [CrossRef]

25. Attabi, S.; Mokhtari, M.; Taibi, Y.; Abdel-Rahman, I.; Hafez, B.; Elmsellem, H. Electrochemical and tribological behavior of surface-treated titanium alloy Ti–6Al–4V. *J. Bio-Tribo-Corros.* **2019**, *5*, 1–11. [CrossRef]

26. El Aatiaoui, A.; Koudad, M.; Chelfi, T.; Erkan, S.; Azzouzi, M.; Aouniti, A.; Savaş, K.; Kaddouri, M.; Benchat, N.; Oussaid, A. Experimental and theoretical study of new Schiff bases based on imidazo (1, 2-a) pyridine as corrosion inhibitor of mild steel in 1M HCl. *J. Mol. Struct.* **2021**, *1226*, 129372. [CrossRef]

27. Benzai, A.; Derridj, F.; Mouadili, O.; El Azzouzi, M.; Kaddouri, M.; Cherrak, K.; Touzani, R.; Aouniti, A.; Hammouti, B.; Elatki, R. Anti-corrosive properties and quantum chemical studies of (benzoxazol) derivatives on mild steel in HCl (1 M). *Port. Electrochim. Acta* **2021**, *39*, 129–147. [CrossRef]

28. Zimila, H.E.; Matsinhe, A.L.; Malayika, E.; Sulemane, Á.I.; Saete, V.N.C.; Rugunate, S.C.; Cumbane, P.J.; Magaia, I.; Munyemana, F. Phytochemical analysis and in vitro antioxidant and antimicrobial activities of hydroalcoholic extracts of the leaves of Salacia kraussii. *Biocatal. Agric. Biotechnol.* **2020**, *30*, 101862. [CrossRef]

29. Sastry, G.M.; Adzhigirey, M.; Day, T.; Annabhimoju, R.; Sherman, W. Protein and ligand preparation: Parameters, protocols, and influence on virtual screening enrichments. *J. Comput.-Aided Mol. Des.* **2013**, *27*, 221–234. [CrossRef]

30. Morris, G.M.; Goodsell, D.S.; Halliday, R.S.; Huey, R.; Hart, W.E.; Belew, R.K.; Olson, A.J. Automated docking using a Lamarckian genetic algorithm and an empirical binding free energy function. *J. Comput. Chem.* **1998**, *19*, 1639–1662. [CrossRef]

31. Charrouf, M.H. Contribution à l'Etude Chimique de l'Huile d'*Argania spinosa*(L.) (Sapotaceae). Ph.D Thesis, Université de Perpignan, Perpignan, France, 1984.

32. Guillaume, D.; Charrouf, Z. Argan oil and other argan products: Use in dermocosmetology. *Eur. J. Lipid Sci. Technol.* **2011**, *113*, 403–408. [CrossRef]

33. Thakur, A.; Kaya, S.; Abousalem, A.S.; Sharma, S.; Ganjoo, R.; Assad, H.; Kumar, A. Computational and experimental studies on the corrosion inhibition performance of an aerial extract of Cnicus Benedictus weed on the acidic corrosion of mild steel. *Process Saf. Environ. Prot.* **2022**, *161*, 801–818. [CrossRef]

34. Tang, L.; Li, X.; Si, Y.; Mu, G.; Liu, G. The synergistic inhibition between 8-hydroxyquinoline and chloride ion for the corrosion of cold rolled steel in 0.5 M sulfuric acid. *Mater. Chem. Phys.* **2006**, *95*, 29–38. [CrossRef]

35. Mu, G.N.; Li, X.; Li, F. Synergistic inhibition between o-phenanthroline and chloride ion on cold rolled steel corrosion in phosphoric acid. *Mater. Chem. Phys.* **2004**, *86*, 59–68. [CrossRef]

36. Hafez, B.; Mokhtari, M.; Elmsellem, H.; Steli, H. Environmentally friendly inhibitor of the corrosion of mild steel: Commercial oil of Eucalyptus. *Int. J. Corros. Scale Inhib.* **2019**, *8*, 573–585. [CrossRef]

37. Jeroundi, D.; Chakroune, S.; Elmsellem, H.; El Hadrami, E.; Ben-Tama, A.; Elyoussfi, A.; Dafali, A.; Douez, C.; Hafez, B. 2,3-(2-alkylthio)-6, 7-bis (2-alkylthio) TTF: A new and green synthetic anti-corrosive inhibitors for mild steel in 1.0 HCl. *J. Mater. Environ. Sci.* **2018**, *9*, 334–344. [CrossRef]

38. Langmuir, I. The adsorption of gases on plane surfaces of glass, mica and platinum. *J. Am. Chem. Soc.* **1918**, *40*, 1361–1403. [CrossRef]

39. Dąbrowski, A. Adsorption—From theory to practice. *Adv. Colloid Interface Sci.* **2001**, *93*, 135–224. [CrossRef]

40. el Hamdani, N.; Fdil, R.; Tourabi, M.; Jama, C.; Bentiss, F. Alkaloids extract of *Retama monosperma* (L.) Boiss. seeds used as novel eco-friendly inhibitor for carbon steel corrosion in 1 M HCl solution: Electrochemical and surface studies. *Appl. Surf. Sci.* **2015**, *357*, 1294–1305. [CrossRef]

41. Afia, L.; Salghi, R.; Bazzi, E.H.; Zarrouk, A.; Hammouti, B.; Bouri, M.; Zarrouk, H.; Bazzi, L.; Bammou, L. Argan hulls extract: Green inhibitor of mild steel corrosion in 1 M HCl solution. *Res. Chem. Intermed.* **2012**, *38*, 1707–1717. [CrossRef]

42. Hammouti, B.; Aouniti, A.; Taleb, M.; Brighli, M.; Kertit, S. L-methionine methyl ester hydrochloride as a corrosion inhibitor of iron in acid chloride solution. *Corrosion* **1995**, *51*. [CrossRef]

43. Bouyanzer, A.; Hammouti, B.; Majidi, L. Pennyroyal oil from Mentha pulegium as corrosion inhibitor for steel in 1 M HCl. *Mater. Lett.* **2006**, *60*, 2840–2843. [CrossRef]

44. Tsuru, T.; Haruyama, S.; Gijutsu, B. Corrosion inhibition of iron by amphoteric surfactants in 2M HCl. *J. Jpn. Soc. Corros. Eng.* **1978**, *27*, 573–581.

45. Mansfeld, F.; Kendig, M.; Tsai, S. Recording and analysis of AC impedance data for corrosion studies II. Experimental approach and results. *Corrosion* **1982**, *38*, 570–580. [CrossRef]

46. Douche, D.; Elmsellem, H.; Anouar, E.H.; Guo, L.; Hafez, B.; Tüzün, B.; El Louzi, A.; Bougrin, K.; Karrouchi, K.; Himmi, B. Anti-corrosion performance of 8-hydroxyquinoline derivatives for mild steel in acidic medium: Gravimetric, electrochemical, DFT and molecular dynamics simulation investigations. *J. Mol. Liq.* **2020**, *308*, 113042. [CrossRef]

47. Mechbal, N.; Belghiti, M.; Benzbiria, N.; Lai, C.-H.; Kaddouri, Y.; Karzazi, Y.; Touzani, R.; Zertoubi, M. Correlation between corrosion inhibition efficiency in sulfuric acid medium and the molecular structures of two newly eco-friendly pyrazole derivatives on iron oxide surface. *J. Mol. Liq.* **2021**, *331*, 115656. [CrossRef]

48. El Guerraf, A.; Titi, A.; Cherrak, K.; Mechbal, N.; El Azzouzi, M.; Touzani, R.; Hammouti, B.; Lgaz, H. The synergistic effect of chloride ion and 1, 5-diaminonaphthalene on the corrosion inhibition of mild steel in 0.5 M sulfuric acid: Experimental and theoretical insights. *Surf. Interfaces* **2018**, *13*, 168–177. [CrossRef]

49. Taşkın, H.; Süfer, Ö.; Attar, Ş.H.; Bozok, F.; Baktemur, G.; Büyükalaca, S.; Kafkas, N.E. Total phenolics, antioxidant activities and fatty acid profiles of six Morchella species. *J. Food Sci. Technol.* **2021**, *58*, 692–700. [CrossRef]

50. Nengroo, Z.R.; Rauf, A. Fatty acid composition and antioxidant activities of five medicinal plants from Kashmir. *Ind. Crops Prod.* **2019**, *140*, 111596. [CrossRef]

51. Martínez-Ceja, A.; Romero-Estrada, A.; Columba-Palomares, M.C.; Hurtado-Díaz, I.; Alvarez, L.; Teta-Talixtacta, R.; Sánchez-Ramos, M.; Cruz-Sosa, F.; Bernabé-Antonio, A. Anti-inflammatory, antibacterial and antioxidant activity of leaf and cell cultures extracts of Randia aculeata L. and its chemical components by GC-MS. *S. Afr. J. Bot.* **2022**, *144*, 206–218. [CrossRef]

52. Getahun, T.; Sharma, V.; Gupta, N. Chemical composition, antibacterial and antioxidant activities of oils obtained by different extraction methods from Lepidium sativum L. seeds. *Ind. Crops Prod.* **2020**, *156*, 112876. [CrossRef]

53. Khowdiary, M.M.; Taha, N.A.; Barqawi, A.A.; Elhenawy, A.A.; Sheta, M.; Hassan, N. Theoretical and experimental evaluation of the anticorrosion properties of new Coumarin's derivatives. *Alex. Eng. J.* **2022**, *61*, 6937–6948. [CrossRef]

54. Lee, H.; Nobe, K. Kinetics and mechanisms of Cu electrodissolution in chloride media. *J. Electrochem. Soc.* **1986**, *133*, 2035. [CrossRef]

55. Deslouis, C.; Tribollet, B.; Mengoli, G.; Musiani, M.M. Electrochemical behaviour of copper in neutral aerated chloride solution. I. Steady-state investigation. *J. Appl. Electrochem.* **1988**, *18*, 374–383. [CrossRef]

56. D'Elia, E.; Barcia, O.E.; Mattos, O.R.; Pébère, N.; Tribollet, B. High-rate copper dissolution in hydrochloric acid solution. *J. Electrochem. Soc.* **1996**, *143*, 961. [CrossRef]

57. Khowdiary, M.; El-Henawy, A.; Shawky, A.; Negm, N. Synthesis and evaluation of novel corrosion inhibitors utilized from the recycling of polyethylene terephthalate polymer: Gravimetric, electrochemical, quantum chemical modeling, and molecular docking studies. *J. Mol. Liq.* **2020**, *320*, 114504. [CrossRef]

58. Elgendy, A.; Nady, H.; El-Rabiei, M.; Elhenawy, A.A. Understanding the adsorption performance of two glycine derivatives as novel and environmentally safe anti-corrosion agents for copper in chloride solutions: Experimental, DFT, and MC studies. *RSC Adv.* **2019**, *9*, 42120–42131. [CrossRef] [PubMed]

59. Azgaou, K.; Damej, M.; El Hajjaji, S.; Sebbar, N.K.; Elmsellem, H.; El Ibrahimi, B.; Benmessaoud, M. Synthesis and characterization of N-(2-aminophenyl)-2-(5-methyl-1H-pyrazol-3-yl) acetamide (AMPA) and its use as a corrosion inhibitor for C38 steel in 1 M HCl. Experimental and theoretical study. *J. Mol. Struct.* **2022**, *1266*, 133451. [CrossRef]

60. Toukal, L.; Belfennache, D.; Foudia, M.; Yekhlef, R.; Benghanem, F.; Hafez, B.; Elmsellem, H.; Abdel-Rahman, I. Inhibitory power of N, N-(1, 4-phenylene) bis (1-(4-nitrophenyl) methanimine) and the effect of the addition of potassium iodide on the corrosion inhibition of XC70 steel in HCl medium: Theoretical and experimental studies. *Int. J. Corros. Scale Inhib* **2022**, *11*, 438–464.

61. Chkirate, K.; Azgaou, K.; Elmsellem, H.; el Ibrahimi, B.; Sebbar, N.K.; Benmessaoud, M.; El Hajjaji, S.; Essassi, E.M. Corrosion inhibition potential of 2-[(5-methylpyrazol-3-yl) methyl] benzimidazole against carbon steel corrosion in 1 M HCl solution: Combining experimental and theoretical studies. *J. Mol. Liq.* **2021**, *321*, 114750. [CrossRef]

62. Jnoff, E.; Albrecht, C.; Barker, J.J.; Barker, O.; Beaumont, E.; Bromidge, S.; Brookfield, F.; Brooks, M.; Bubert, C.; Ceska, T. Binding mode and structure–activity relationships around direct inhibitors of the Nrf2–Keap1 complex. *ChemMedChem* **2014**, *9*, 699–705. [CrossRef]

63. Tao, Z.; Zhang, S.; Li, W.; Hou, B. Corrosion inhibition of mild steel in acidic solution by some oxo-triazole derivatives. *Corros. Sci.* **2009**, *51*, 2588–2595. [CrossRef]